MagTrack: Enabling Safe Driving Monitoring with Wearable Magnetics

Hua Huang, Hongkai Chen, and Shan Lin

Department of Electrical and Computer Engineering, Stony Brook University

Stony Brook, NY, USA

{hua.huang,hongkai.chen,shan.x.lin}@stonybrook.edu

ABSTRACT

"Hands on the wheel, eyes on the road" is the central guideline of safe vehicle driving practices. Many advanced driver assistance systems can effectively detect abnormal vehicle motions. However, these systems often leave insufficient time for drivers to respond to complex road situations, especially when the drivers are distracted. To reduce accidents, it is essential to detect whether a driver complies with safe driving guidelines in real time and provide warnings early before any dangerous maneuvers occur. There are vision-based driver distraction monitoring systems which rely on cameras in high-end vehicles, but their performances are heavily constrained by visibility requirements. In this paper, we present MagTrack, a driver monitoring system that is based on tracking magnetic tags worn by the user. With a single smartwatch and two low-cost magnetic accessories: a hand magnetic ring and a head magnetic eyeglasses clip, our system tracks and classifies a driver's bimanual and head movements simultaneously using both analytical and approximation sensing models. Our approach is robust to driver's postures, vehicles, and environmental changes. We demonstrate that a wide range of activities can be detected by our system, including bimanual steering, visual and manual distractions, and lane changes and turns. In extensive road tests with 500+ instances of driving activities and 500+ minutes of road driving with 10 subjects, MagTrack achieves 87% of precision and 90% of recall rate on the detection of unsafe driving activities.

CCS CONCEPTS

• **Human-centered computing** → **Ubiquitous and mobile computing**.

KEYWORDS

Driver Assistance System; Wearable Magnetics; Smartwatch Sensing

1 INTRODUCTION

Distracted driving causes 9 fatalities and 1,071 injuries in the U.S. each day [18], and drivers are at fault for 94% of all car collisions surveyed by the National Highway Traffic Safety Administration (NHTSA) [58]. Most of these errors result from the driver's failure to comply with safe driving guidelines, including manual distractions (e.g., one hand off wheel), visual distractions (e.g., eyes off road), unsafe turn and lane change (e.g., failure to check blind spot), and incorrect steering techniques (e.g., one-hand steering, hand-over-hand steering). We can prevent many accidents if these unsafe driving behaviors are automatically detected in real-time.

Unfortunately, existing technologies for driver activity monitoring have their limitations. Some advanced driver assistance systems can effectively detect abnormal vehicle motions, then warn the drivers of impending collisions [22], lane deviations [33], and aggressive steering [6, 9, 29]. However, they often leave insufficient time for the drivers to respond to complex road situations, especially when the drivers are distracted [2, 19, 34]. Therefore, it is important to detect unsafe driving activities early before any dangerous maneuvers occur.

Camera based systems that can detect visual distractions and drowsy driving have been developed and deployed in high-end vehicles, but they are constrained by visibility requirements, and unable to monitor abnormal hand movements, including manual distractions or aggressive steering. Wearable technologies have been used to monitor driving activity. For example, previous research used inertial measurement units (IMUs), commonly found on smartwatches, to detect erratic steering wheel movements [6] and manual distractions [7], but these solutions are limited to the detection of the hands where smartwatches are worn. Therefore, the development of reliable, robust, and low-cost technologies to monitor various driver activities is desirable.

In this paper, we present Magtrack, a driving monitoring system using a novel, different approach. Since small and cheap permanent magnets produce their own persistent magnetic fields without any power consumption, they can serve as active tracking tags in short range. So we embed off-the-shelf magnets into various user-friendly accessories, such as buttons, rings, gloves, wristbands, headbands, eyeglasses, earphones, ear clips, etc. These accessories, if worn by a user, can provide magnetic signals that convey rich information about the user's movements. Since driving activities consist of coordinated hand and head movements, we use two wearables, specifically a magnetic ring worn on one hand and a magnetic eyeglasses clip.

To track these tags, the driver wears a smartwatch on the opposite hand to measure the magnetic field, and recognize 3D hand and head motions based on driving activity models. Previous research on magnetic tag tracking usually use two or more magnetometers to track each target [10, 12, 16, 23, 60]. The reason is that a single magnetic tag has six degrees of motion freedom, and two three-axis magnetometers are required to uniquely identify its location and orientation. It is very challenging to track two targets with just one magnetometer. To tackle this problem, we identify that most safe driving activities consist of coordinated and deterministic hand and head movements. As a result, each tag has its specific motion patterns and constraints, which provides a unique opportunity for us to differentiate the signals generated from the two tags and even track their concurrent motions. Based on these observations, we develop motion models and tracking algorithms to recognize different driving activities.

We validated our sensing and activity recognition algorithms with different drivers, different types of cars, under different road conditions. Particularly, we demonstrated that our solution is able to adapt to gesture variations and geometric magnetic field changes during road tests. Moreover, by analyzing the likely motions associated with unsafe driving behaviors, we design real-time monitoring algorithms to detect i) manual and visual distractions, when the driver takes either hand off the steering wheel or spends too much time with eyes off the road; ii) incorrect steering control, when the driver makes abrupt or improper steering motions; and iii) unsafe lane changing and turning when the driver fails to perform a shoulder check on the blind spot and switch on turn signals before steering. MagTrack can benefit many people, including night commuters, long-distance drivers, novice drivers, and drivers with Attention Deficit and Hyperactivity Disorder (ADHD)[55, 61].

We summarize the contributions of this work as the following:

- We build a driver monitoring system that reliably monitors a driver's two hands and head motions in real-time. Our system detects a wide range of unsafe driving activities including manual and visual distractions, unsafe turning and lane changing, and incorrect steering control. It is robust against different types of vehicles and environmental settings.

- To facilitate fine-grained tracking in a small space, we use battery-free off-the-shelf magnets to design user-friendly magnetic accessories for the drivers. These active wearable tags provide additional signals that convey rich position and motion information about a driver's posture and motion.

- We design a novel sensing algorithm that tracks the drivers' magnetic wearables with a single magnetometer on the drivers' smartwatch. As each wearable has its unique motion patterns and constraints, our algorithm is able to differentiate the signals generated from the two tags and even track their concurrent motions. Based on the tracking results, we further develop a machine learning based algorithm to detect different driving activities. Our approach can go beyond the driver monitoring application.

- In extensive road tests with 500+ instances of different driving activities and 500+ minutes driving time from 10 subjects, MagTrack successfully achieves 87% of precision and 90% of recall rate on unsafe driving activities detection.
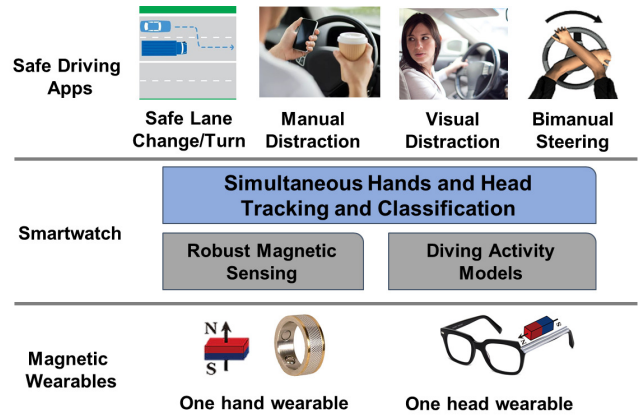

Figure 1: System Architecture of MagTrack

2 OVERVIEW

2.1 Safe Driving Compliance Problem

Driving activities require coordinated hand and head movements, because the drivers need to assess the surrounding environment and control the vehicle accordingly. Safe driving guidelines in driver's manuals define the correct movements (e.g., positions, timings, and sequences). Adherence to these guidelines minimizes the risks of driving. However, many drivers fail to comply with these rules, especially when they are distracted or tired. Here, we define some of the most common unsafe driving behaviors: (i) manual distraction: a driver takes either hand off the steering wheel for other activities such as making phone calls or eating; (ii) visual distraction: a driver takes eyes off the road and turns head to scenery or advertisement signs, or even chats with passengers. (iii) incorrect steering control: a driver is holding the steering wheel at the wrong positions, or steering the wheel using improper or aggressive ways; and (iv) unsafe lane changing/turning: a driver fails to turn their head to check the blind spots and the side mirror (or traffic from other directions at the intersection) before steering the car to change lane or turn.

We can see that these practices boil down to combinations of a few basic types of hand and head gestures. The basic driving hand gestures include holding and steering movements. Holding the wheel requires a driver to put both hands on the steering wheel at the correct positions. Taking either hand off the wheel for too long increases safety risks. Steering movements involve coordinated bimanual hand movements to turn the wheel. The head gestures include turning head leftward, rightward, downward with an angle. To monitor the driving activities, it is essential to capture all these hand and head gestures.

2.2 System Design Overview

The system architecture of MagTrack is shown in Figure 1. MagTrack consists of three layers:

- Magnetic wearable accessories. MagTrack uses them to track different body parts of the driver. We attach a block magnet that measures $5cm \times 2.5cm \times 1.25cm$ to the driver's finger, and a column-shaped magnet with a height of $11cm$ and radius $4mm$ to a pair of eyeglasses at the driver's left temple.

It is possible to customize the magnetic wearables with different form factors and types, such as buttons, rings, gloves, wristbands, headbands, eyeglasses, earphones, ear clips, etc.

- A smartwatch. To monitor driving activities, we put the smartwatch on the opposite hand to the one with the magnet. The main challenge of our approach is to use a single magnetometer on the smartwatch to track two magnetic wearables. We address this challenge by developing a novel sensing algorithm to differentiate magnetic signals generated from two magnets, and track them simultaneously.

- Safe driving apps. These apps recognize different driving activities, and issue warnings to the driver if they detect violations of safe driving guidelines. These apps can be configured based on the driver's driving habits, e.g., driving posture. They can also take other factors such as traffic and road conditions into account, if such information is available.

3 HAND AND HEAD TRACKING

In this section, we focus on monitoring the movements of the magnetic tags attached to the driver's hand and head, using the smartwatch magnetometer. When the driver's hands are holding the steering wheel, their motions are constrained within a circle. Similarly, the driver's head is constrained by the car seat configuration. We construct motion and sensing models for these hand and head movements. Based on these models, we design a Simultaneous Tracking and Classification (STC) algorithm to track the magnetic tags. The STC framework consists of a bank of parallel running Kalman filters that track different magnetic tags and motion types, including hand steering motions, head turn motions, and concurrent hand and head motions. The STC algorithm firstly identifies the most likely motion type (hand, head, or concurrent motions), and then estimates the corresponding motion track.

3D rotation. In the development of the sensing models, the 3D rotation operations of vectors are used extensively. The 3D rotation around an axis A for angle β can be represented using a matrix $R(A, \beta)$ [44], which is shown in the following equation:

$$R(A, \beta) = \begin{bmatrix} tu_x^2 + C & tu_x u_y - Su_z & tu_x u_z + Su_y \\ tu_x u_y + Su_z & tu_y^2 + C & tu_y u_z - Su_x \\ tu_x u_z - Su_y & tu_y u_z - Su_x & tu_z^2 + C \end{bmatrix}, \quad (1)$$

where $A = [u_x, u_y, u_z]^T, C = \cos(\beta), S = \sin(\beta), t = 1 - C$.

3.1 Hand Steering Motion Modeling

In this subsection we describe how to use our Kalman filtering model to track the right hand motions on the steering wheel. A Kalman filter includes a State Transition Model and a Measurement Model. The State Transition Model contains a state variable vector, which describes the right hand position and posture, and a state transition matrix, which describes how the state variable vector evolves over time. We then introduce the Measurement Model, which describes how the right hand position and posture influence the sensor measurements. Based on above models, we are able to use the Unscented Kalman filter [67] to track the right hand motions.

State Transition Model. We use θ_1 to represent the user's right hand holding position. As illustrated in Figure 2, θ_1 is the angle between the hand and the 3 o'clock position of the steering wheel.
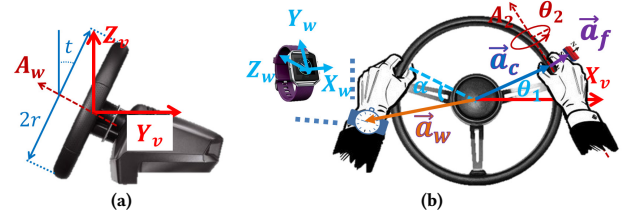

Figure 2: Steering Motion Model

We use θ_2 to represent the user's hand posture, which describes how the driver holds the steering wheel. As illustrated in Figure 2, the driver's hand can rotate around the steering wheel tube with an angle θ_2. We set θ_2 to zero when the north pole direction of the magnetic tag lies on the steering wheel plane and points to the centrifugal direction.

We also include the change rates, $\dot{\theta}_1$ and $\dot{\theta}_2$ into the state variable vector. The benefit is that the tracker will have quicker responses to the system variable changes. By definition, for time step k, we have $\theta_i(k) = \theta_i(k - 1) + \Delta T * \dot{\theta}_i(k - 1)$ for $i = 1, 2$, where ΔT denotes the time interval between two time steps. Writing them into matrix form, we have $X^s(k) = F^s \cdot X^s(k - 1)$, where the state variable vector $X^s(k)$ and state transition matrix F^s are defined in the following equations:

$$X^s(k) = \begin{bmatrix} \theta_1(k) \\ \dot{\theta}_1(k) \\ \theta_2(k) \\ \dot{\theta}_2(k) \end{bmatrix}, F^s = \begin{bmatrix} 1 & \Delta T & 0 & 0 \\ 0 & 1 & 0 & 0 \\ 0 & 0 & 1 & \Delta T \\ 0 & 0 & 0 & 1 \end{bmatrix}. \quad (2)$$

Measurement Model. Next we construct the measurement model for hand steering motions. Our goal is to find the analytical function that maps the hand holding position and posture, represented by θ_1 and θ_2, to and the magnetic field measurements on the smartwatch. The field of the hand magnetic tag is determined by its position relative to the sensor, $\vec{a}_t$, and magnetic moment $\vec{m}$, which is a vector describing the dipole strength and direction. In what follows, we analyze how the changes in θ_1, θ_2 influence the values of $\vec{a}_t$ and $\vec{m}$. When $\vec{a}_t$ and $\vec{m}$ are obtained, we compute the estimated magnetic field using the standard field distribution function.

As shown in Figure 2, we use r to denote the radius of the steering wheel, and t the tilt angle of the steering wheel. The vehicle coordinate frame $X_v - Y_v - Z_v$ is defined as follows: Z_v is pointing vertically upwards; Y_v is pointing horizontally forwards; X_v is perpendicular to both Y_v and Z_v, and is pointing right.

● *Hand Magnetic Tag Position* . We decompose the vector from the magnetic tag to the smartwatch sensor, denoted by $\vec{a}_t$, into three components:

$$\vec{a}_t = \vec{a}_w - \vec{a}_c(\theta_1) - \vec{a}_f(\theta_1, \theta_2). \quad (3)$$

$\vec{a}_w$, the orange vector in Figure 2, is the vector from the center of the steering wheel to the smartwatch magnetometer when the driver is holding the steering wheel. The position of the watch depends on the driver's hand holding position and personal holding habit. We compute an estimate of $\vec{a}_w$ during the calibration process. In this section, we consider the case when the driver's left hand is holding the steering wheel without moving. In Section 5, we will provide algorithms to detect the driver's left hand motions.
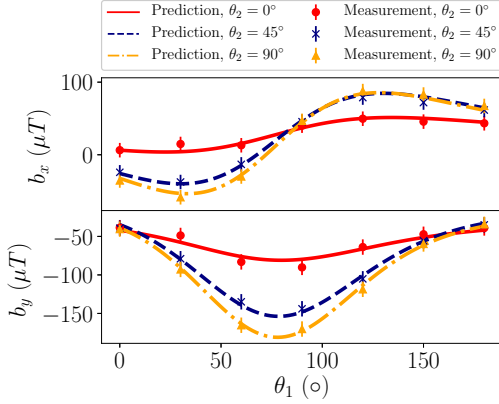
Figure 3: Magnetic Measurements vs. Model Estimations

The vector $\vec{a}_c$ is the blue vector in Figure 2. The value of $\vec{a}_c$ is determined by the holding position θ_1. When θ_1 changes, $\vec{a}_c$ can be viewed as a vector rotating around rotation axis A_w of the steering wheel, which has a tilt angle t. We derive the expression of $\vec{a}_c$ by rotating from its initial position. Specifically, $\vec{a}_c(\theta_1) = R_{A_w}(\theta_1) * r * [1, 0, 0]^T$, where $R_{A_w}(\theta_1)$ represents a 3D rotation around axis A_w with angle θ_1, as defined in Equation 1. r is the radius of the steering wheel. The expressions for $\vec{A}_w$ and $\vec{a}_c(\theta_1)$ are as follows:

$$\begin{aligned} \vec{A}_w &= [0, -\cos t, \sin t]^T, \\ \vec{a}_c(\theta_1) &= R(A_w, \theta_1) * r * [1, 0, 0]^T. \end{aligned} \quad (4)$$

Next we analyze $\vec{a}_f$ in Equation 3, illustrated as the purple vector in Figure 2. The thickness of the driver's finger and the shape of the magnetic tag determine the length of $\vec{a}_f$, denoted by l. Intuitively, $\vec{a}_f$ can be viewed as a vector rotating around axis $\vec{A}_2$ by an angle θ_2. $\vec{A}_2$ is a unit vector perpendicular to both $\vec{a}_c$ and $\vec{A}_w$, so we can compute the value of $\vec{A}_2$ using the cross product between $\vec{A}_w$ and $\vec{a}_c$. When $\theta_2 = 0$, $\vec{a}_f$ is parallel to $\vec{a}_c$, i.e., $\vec{a}_f(\theta_1, 0) = l/r * \vec{a}_c(\theta_1)$. Therefore, we compute $\vec{a}_f(\theta_1, \theta_2)$ by rotating the vector $\vec{a}_f(\theta_1, 0)$ around the axis $\vec{A}_2$ by an angle θ_2, as shown in the following equation:

$$\begin{aligned} \vec{A}_2 &= \vec{A}_w \times \vec{a}_c(\theta_1), \\ \vec{a}_f(\theta_1, \theta_2) &= \frac{l}{r} * R(A_2, \theta_2) * \vec{a}_c(\theta_1). \end{aligned} \quad (5)$$

Finally, we can use $\vec{a}_c$, $\vec{a}_f$ and $\vec{a}_w$ to compute the magnetic tag relative position $\vec{a}_t$ using Equation 3.

• *Hand Magnetic Tag Orientation.* The direction of the magnetic tag's north pole is represented by $\vec{m}$. In our case, $\vec{m}$ has the same direction with vector $\vec{a}_f$, shown in Figure 2. $\vec{m}$ is be computed by rotating its initial value $\vec{m}(0, 0)$ around axes $\vec{A}_w$ and $\vec{A}_2$ for angles θ_1 and θ_2 consecutively. When $\theta_1 = \theta_2 = 0$, $\vec{m} = [1, 0, 0]^T$. The vector $\vec{m}$ is computed as follows:

$$\vec{m} = R(A_w, \theta_1) * R(A_2, \theta_2) * [1, 0, 0]^T. \quad (6)$$

In this equation, $R_{A_w}(\theta_1)$ and $R_{A_2}(\theta_2)$ represent the 3D rotation operations defined in Equation 1, and rotation axes $\vec{A}_2$ and $\vec{A}_w$ are defined in Equation 4 and 5.

Magnetic Field Estimation. Based on the estimates of $\vec{a}_t$ and $\vec{m}$ described from Equation 3 to 6, we can analytically calculate the magnetic field $\vec{B}$:
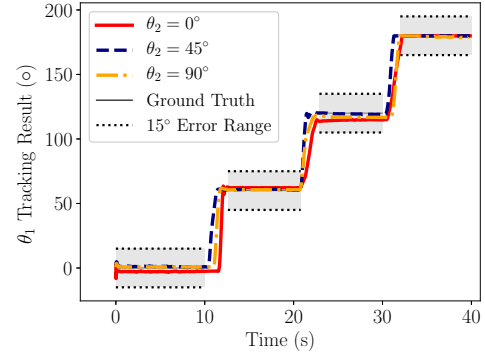

Figure 4: Right Hand Tracking

$$\vec{B} = H^s(\theta_1, \theta_2) = \frac{|M|\mu}{4\pi|\vec{a}_t|^3} \left[\frac{3\vec{a}_t\vec{a}_t^T}{|\vec{a}_t|^2} - \mathbf{I}_3 \right] \vec{m}, \quad (7)$$

where $|\vec{a}_t|$ is the norm of $\vec{a}_t$, $|M|$ is a constant describing the strength of the magnet, and μ is a constant representing the magnetic permeability of the environment. We plot the theoretical values $\vec{B}$ and the actual measurements $\vec{b}$ in Figure 3 when the driver is holding different positions with different postures. Our model accurately predicts sensor measurements even when holding position θ_1 varies from $0°$ to $180°$ and wrist angle θ_2 varies from $0°$ to $90°$.

With the definition of state transition model (Equation 2) and measurement model (Equation 7), we can track the values of the state variables, holding position θ_1 and posture θ_2, using the Kalman filtering algorithm. Since the measurement model is nonlinear, we select the Unscented Kalman filtering algorithm [67], which has low computation cost and the ability to handle nonlinear Kalman filtering models. A sample tracking result is shown in Figure 4. During the experiment, the driver changes the steering wheel holding position θ_1 slowly, and the ground truth holding positions are represented by the black thin line. We repeat this test for three times with different holding postures θ_2, which ranges between $0°$ and $90°$. We can see that the θ_1 tracking results, represented by thick lines in Figure 4, closely follow the ground truths.

To calibrate the right hand tracking algorithm, we need to know three parameters r, t, and $\vec{a}_w$ in Figure 2. It is possible to directly measure these parameters, but we find it easier to adopt the Maximum Likelihood Parameter Estimation (MLPE) approach. MLPE can search for the most likely parameters such that the magnetic field computed by the sensing model closely matches the measurements [70]. Specifically, the driver needs to hold the steering wheel with their right hand with different positions θ_1 and postures θ_2. The system records the magnetic sensor measurements together with the ground truth values of θ_1, θ_2. Then we use MLPE to estimate the values of r, t, and $\vec{a}_w$, such that the model predictions are closest to the actual magnetic sensor measurements.

3.2 Head Motion Modeling

Next, we present the Kalman filtering models for head motion monitoring. As described earlier, we attach a magnet to the driver's eyeglasses and use the smartwatch magnetometer to detect its motions. The primary challenge is that the long distance from the tag
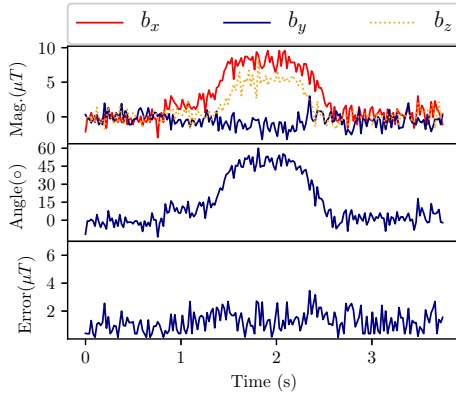
Figure 5: Magnetometer Measurements, Head Angle, and Estimation Error for Left Head Turn

to the magnetometer causes a low signal-to-noise ratio because the magnetic field strength at the magnetometer is relatively weak. As a result, it's difficult to construct an exact analytical measurement model for the head magnetic tag. To address this challenge, we first divide head motions into three types: left turn, right turn, and nodding, then construct a separate Kalman filter to track each of them. This way we reduce the complexity for tracking head turns for each direction, so that an approximate linear measurement model can be used. We firstly present the Kalman filter, denoted by KF^l, which tracks the left head turn motions, in Equation 8. The Kalman filter designs for other directions are similar.

$$KF^l : \quad X^l(k) = \begin{bmatrix} \gamma_l(k) \\ \dot{\gamma}_l(k) \end{bmatrix}, F^l = \begin{bmatrix} 1 & \Delta T \\ 0 & 1 \end{bmatrix}, \quad (8)$$
$$\vec{B}^l(k) \approx H^l(\gamma_l(k)) = \vec{a}_0 + \vec{a}_1 * \gamma_l(k).$$

The Kalman filter KF^l consists of a State Transition Model and a Measurement Model. The state variable $X^l(k)$ contains the left head turn angle γ_l ranging from $0°$ to $90°$. When the driver is facing forwards, we set γ_l zero. To facilitate the tracking, we further include the head angle change rate $\dot{\gamma}_l$ into the state variable. By definition, we have $\gamma_l(k) = \gamma_l(k-1) + \Delta T * \dot{\gamma}_l(k-1)$. Taking it into matrix form, we have $X^l(k) = F^l \cdot X^l(k-1)$, where $X(k)$ and F^l are defined in the first line of Equation 8.

We use the linear approximation technique to create the measurement model for the head left turn. When the driver's head turns leftwards, the 3D magnetic field measurements $\vec{B}^l$ can be regarded as a function of the left head turn angle γ_l. Instead of finding the exact expression of this function, we use linear approximation, i.e., $\vec{B}^l \approx \vec{a}_0 + \vec{a}_1 \gamma_l$. The values of $\vec{a}_0$ and $\vec{a}_1$ are estimated in the calibration process, which will be described at the end of this subsection.

After the Kalman filtering model KF^l is defined, we can use the classical linear Kalman filter to estimate the head left turn angle $\gamma_l(k)$ [69]. We plot the tracking result in the middle row of Figure 5. To validate the measurement models $H^l()$, we compute the model estimation error $e_k = |\vec{B}(k) - H^l(\gamma_l(k))|$. The results are shown in the third row in Figure 5. We can see that the norms of the estimation errors are almost always smaller than $3\mu T$.

Using the same technique used to construct the left head turn Kalman filter KF^l, we can also construct the Kalman filters for right

head turns and down head turns, which are represented by KF^r, KF^d.

To calibrate the head tracking algorithm, we need to know the values of $\vec{a}_0$ and $\vec{a}_1$ in Equation 8. During the calibration, the driver turns head to the left, right and down once, and the sensor measurements are recorded, denoted by $[B_1, B_2, ..., B_n]$. $\vec{a}_0$ is estimated by computing the mean of the measurements B for the first few seconds when the driver faces forwards and the head angle is zero. When the driver turns head to the maximal angle, about $90°$, the value of $|B_k - \vec{a}_0|$ takes the maximal value. We then use a standard linear regression technique to estimate the value of $\vec{a}_1$.

3.3 Simultaneous Tracking and Classification

Concurrent Motion Modeling. In some cases, the driver moves their hand and head at the same time. For example, while steering at an intersection, the driver may also turn their head to check for pedestrians. Intuitively, when both magnetic tags move simultaneously, the impact on the sensor measurements is a superposition of the influence from each tag. We use separate Kalman filters to monitor concurrent steering and head turning motions, i.e., the driver turns head left or right while steering the wheel with their right hand. We define the measurement model as the sum of the measurement models for hand and head motions. The Kalman filter for concurrent steering and head left turn motions, KF^{sl} is shown below.

$$KF^{sl} : \quad \begin{aligned} X^{sl} &= \{\theta_1, \theta_2, \gamma_l\}, F^{sl} = \mathbf{I}_{3\times3}, \\ B^{sl} &= H^{sl}(\theta_1, \theta_2, \gamma_l) = H^s(\theta_1, \theta_2) + H^l(\gamma_l) - \vec{a}_0, \end{aligned} \quad (9)$$

where $H^s(\theta_1, \theta_2)$ and $H^l(\gamma_l)$ are the measurement models for hand steering and head turn motions defined in Equation 7 and 8, respectively. To reduce the error detections that confuse individual motions with concurrent motions, we add an constraint that θ_1 and γ_l be larger than certain thresholds, i.e., $|\theta_1| > T_{\theta_1}$ and $|\gamma_l| > T_{\gamma_l}$. This way, the Kalman filter KF^{sl} for concurrent motions becomes active only when both magnetic tags have large motions. On the other hand, if only one magnetic tag is moving, the separate Kalman filters KF^s or KF^l will be selected.

Simultaneous Tracking and Classification. Using the Kalman filtering models, KF^i, where $i = s, l, r, d, sl, sr$, which corresponds to right hand steering, head left turn, head right turn, head down turn, concurrent steering and head left turn, and concurrent steering and head right turn, hand and head motions can be recognized and tracked in real time. Based on the tracking results of these parallel Kalman filters, the STC framework can choose the most likely motion type using the Bayesian rule. The STC is described in Algorithm 1. The input of the algorithm is the magnetic sensor measurements within a time window, represented by $\{B(1), B(2), ..., B(W)\}$. The algorithm output is the most likely motion type c, and the corresponding tracking results $\{X^c(1), X^c(2), ..., X^c(W)\}$.

Given the sensor measurement $B(k)$, the algorithm runs all the 6 parallel Kalman filters, as shown in Line 3. Line 4 and 5 represent the Kalman filters' prediction and update steps, which estimate of the state variable $X^i(k)$ for the motion class i. We use an Unscented Kalman filter [67] for hand steering and concurrent motion tracking, and a classical linear Kalman [69] filter for head turn

Algorithm 1 *Simultaneous Tracking and Classification*

Input: Magnetometer Measurement: $B(k), k = 1, 2, ..., W$
Output: Motion Type: c, Tracking Result: $X^c(k), k = 1, 2, ..., W$
1: $count_i \leftarrow 0$ for all Motion Class i
2: **for** Time Step $k = 1 : W$ **do**
3:     **for** Motion Class $i = 1 : N$ **do**
4:         $\tilde{X}^i(k) \leftarrow F \cdot X^i(k-1)$
5:         $X^i(k) \leftarrow update(B(k), \tilde{X}^i(k))$
6:         $\delta_k^i \leftarrow B(k) - H^i(X^i(k))$
7:         $P(B(k)|i) \leftarrow \frac{1}{(2\pi)^{3\sigma/2}} exp\{-\delta^i(k)^T \delta^i(k)/(2\sigma)\}$
8:         $P(i|B(k)) = \frac{P(B(k)|i)P(i)}{\sum_{j=1}^s P(B(k)|j)P(j)}$
9:         Normalize $P(i|B(k))$
10:         **if** $P(i|B(k)) > T$ **then**
11:             $count_i + +$
12:         **end if**
13:     **end for**
14: **end for**
15: $c \leftarrow \arg \max_i (count_i)$
16: **return** $c, \{X^c(1), X^c(2), ..., X^c(W)\}$

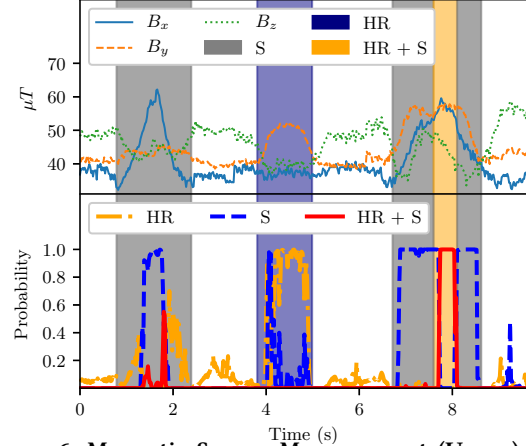**Figure 6: Magnetic Sensor Measurements(Upper) and Motion Class Likelihood (Lower).**

motion monitoring. To calculate the error covariance matrices, we use methods standard in Unscented and classical Kalman filters. Greater details can be found in [67, 69]. In Line 6, the post-fit measurement residue $\delta^i(k)$ is computed, which is the difference between ground-truth measurement $B(k)$ and the post-fit measurement estimate $H(X^i(k))$. We assume the sensor measurements contain white noises $V \sim N(0, \sigma^2)$, where σ^2 is the variance. Therefore, we can compute the conditional probability $P(B(k)|i)$ using the Gaussian distribution equation described in Line 7. Then we calculate the posterior probability $P(i|B(k))$ that represents the likelihood of the motion class i given measurement $B(k)$, using the Bayes principle described in Line 8. $P(j)$ is the prior probability of occurrence of each motion class. We then normalize the probability $P(i|B(k))$ so that $\sum_j P(j|B(k)) = 1$. A significance test is conducted by comparing $P(i|B(k))$ with a threshold T to ensure sufficient confidence in motion probability. We finally select the most likely motion class c within the time window W such that $P(c|B(k))$ has values greater than T for the most number of time steps. The motion class c and the corresponding tracking results $\{X^c(1), X^c(2), ..., X^c(W)\}$ will be returned.

In Figure 6, sample motion classification results are shown. Between second 1 and 2.2, the driver is steering the wheel (S). Between second 3.8 and 5, the driver is turning head rightwards (HR), and between second 6.8 and 8.8, the driver is steering the car, and turns head rightwards briefly at second 8 (HR+S). We can see that the STC algorithm correctly recognizes the correct motions types by raising the motion class likelihood to close to 1.

4 ROBUST MAGNETIC SENSING

Sensor Coordinate Frame Rotation. During driving, the driver's left hand (with smartwatch) can move slightly without steering due to car vibration or holding position change. When the sensor rotates, the measurement changes accordingly. We address this

issue by rotating the magnetic sensor measurements based on the gravity sensor measurement $g = [g_x, g_y, g_z]^T$. The pitch angle p and roll angle r, and the estimate of rotation matrix R_t can be computed as:

$$
\begin{aligned}
p &= \arctan(g_y/\sqrt{g_x^2 + g_z^2}), \\
r &= \arctan(-g_x/g_z), \\
R_t &= R(Y_w, p) * R(X_w, r),
\end{aligned} \tag{10}
$$

where $R(Y_w, p)$ and $R(X_w, r)$ represent rotation operations around axis Y_w and X_w for angle p and r, respectively. The axes Y_w and X_w are illustrated in Figure 2a and the definition of rotation function $R(\cdot, \cdot)$ is shown in Equation 1. With R_t, we calculate the rotated magnetometer measurement $B^R = R_t * B$, which will be used in right hand and head turn motion tracking.

Note that we haven't accounted for the yaw angle variation in the smartwatch, i.e., the rotation around vertical axis Z_v in Figure 2a. Our observation is that when the driver is holding the steering wheel, the yaw angle change of the watch is usually small enough to ignore. When the driver takes the hand off the steering wheel, we design an off-wheel detection algorithm to detect this situation in the following sections.

Geomagnetic Field Reduction. When the car changes its moving direction, the geomagnetic field influences the magnetometer measurements. In Figure 7, we plot the magnetic sensor measurements when the car has different orientations (measured by GPS, plotted with thick orange dashed line). We can see that the horizontal components of the geomagnetic field, i.e., b_x and b_y, change according to the moving directions, while the vertical component b_z remains stable. We reduce the influence of the geomagnetic field using the following strategy. We measure the moving direction d of the car using the GPS sensor on the smartphone. Then we estimate the horizontal components of the geomagnetic field using the following equation:

$$
B^{geo}(d) = |b_h| \begin{bmatrix} \cos(d + \delta) \\ \sin(d + \delta) \\ 0 \end{bmatrix} = R(Z_v, \delta) \begin{bmatrix} \cos d \\ \sin d \\ 0 \end{bmatrix}, \tag{11}
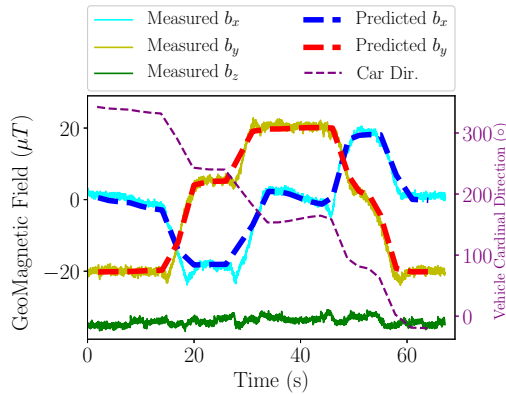$$

Figure 7: Geomagnetic Field Estimation.

where $|b_h|$ denotes the strength of the horizontal component of the geomagnetic field, and δ represents the angle on the horizontal plane between geomagnetic north and the geographic north. $R(Z_v, \delta)$ represents the rotation around Z_v (shown in Figure 2) for angle δ. We estimate the matrix $R(Z_v, \delta)$ using linear regression as follows. The car drives in different directions, which is achieved by driving in a rectangle route. Using the GPS sensor, the ground truth moving directions $d_1, d_2, ..., d_l$ are recorded. In the meanwhile, the smartwatch magnetic sensor measurements $b_1, b_2, ..., b_l$ are also recorded. Then a linear regression is used to find the matrix $R(Z_v, \delta)$ such that $R(Z_v, \delta)[\cos(d_i), \sin(d_i), 0]^T \approx [b_{ix}, b_{iy}, b_{iz}]^T, \forall i$.

Prediction results based on Equation 11 are the plotted with dashed lines in Figure 7. We can see that the predictions (dashed lines) closely follow the magnetometer measurements (thick lines). We use this approach to remove the disturbance of the geomagnetic field before estimating hand holding positions and head turn angles.

5 STEERING CONTROL MONITORING

Left Hand Position Tracking. As illustrated in Figure 2a, we use α to represent the left hand holding position of the driver. We set $\alpha = 0$ when the driver is holding the 9 o'clock position. We use the smartwatch inertia sensors to track left hand position on the steering wheel. The Android wear provides an API to get an estimate the direction of gravity in the smartwatch's coordinate frame, denoted by g, in real time. Then we use the polynomial regression technique to derive the function $f(\cdot)$ such that $g_i = f_i(\alpha), i = x, y, z$. Then we estimate the steering wheel holding position α with the gravity sensor measurements $g = [g_x, g_y, g_z]^T$ by solving the following optimization problem:

$$\underset{\alpha}{minimize}: \quad J = \sum_{i=x,y,z} |g_i - H_i(\alpha)|^2, \quad (12)$$
$$s.t. \quad -60^\circ \leq \alpha \leq 120^\circ.$$

We use a standard convex optimization solver to compute the optimal value for α. We find that when the polynomial regression has an order n greater than 3, we achieve a left hand tracking accuracy of about 10°. Once the system detects that the left hand holding position is close to the 9 o'clock position, i.e., $\alpha \approx 0$, right hand and head sensing algorithms will be invoked. We also test the robustness of this algorithm against the acceleration and deceleration. We record the sensor measurements while driving along roads with speeds ranging from 0 to 55 miles per hour. We find that left hand tracking is robust to ordinary car speed changes.
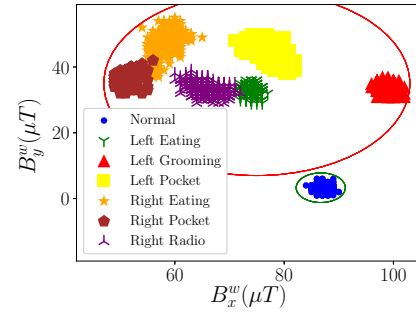

Figure 8: Magnetometer Measurements with Different Manual Activities.

Off-Wheel Detection. In the previous sections, we focus on driver motion tracking when the driver is holding the steering wheel with both hands. However, the driver can take the hands off the steering wheel from time to time, either for ordinary activities like controlling the radio or distracting activities such as texting. Furthermore, it's possible that the driver holds the steering wheel using improper ways, such as one-hand hold or "fingertip" hold. In this section, our goal is to design an algorithm to detect if either hand is off the steering wheel, or if an improper steering wheel holding technique is used.

We use the smartwatch's magnetometer, gravity sensor, and accelerometer measurements within a time window to conduct off-wheel detection. The first feature we use is the mean of the magnetometer measurements within the time window. When the driver takes either hand off the steering wheel, the magnetometer measurements change accordingly because the relative position and orientation between the magnetic tag and the smartwatch change. When the driver conducts different activities using either hand, the smartwatch magnetic sensing measurements are plotted in Figure 8. We can see that the sensor measurements for different activities form distinguishable clusters.

The second feature is the mean of the gravity sensor measurements within a time window. We design the third detection feature based on the linear accelerometer, which can recognize the vertical motions when the driver takes the hand off the steering wheel. Linear acceleration, which is defined as the gross acceleration subtracting the gravity, is denoted by $a(t)$. To obtain the acceleration along the vertical direction, we take the dot product between $a(t)$ and the gravity sensor measurement $g(t)$, i.e., $a_{vert} = a(t) \cdot g(t)/|g(t)|$. The third feature is defined as the variance of a_{vert} within the time window.

To simplify the training process, we select the one-class Support Vector Machine (SVM) algorithm [68]. A one-class SVM classifier is trained using data generated by the sensing models for the two hands and the head. After training, the algorithm compares features from new sensor measurements with the training data. If the new features are too different, the algorithm declares it to be out of class, which indicates abnormal steering wheel holding or off-wheel motions. Specifically, we iterate through all the normal possible motion states of the hand and head, i.e., θ_1, θ_2, for hand holding on the steering wheel; and γ for different head turn directions. Using the magnetic sensor measurement models $H^s()$ and $H^i(), i = l, r, d$, we compute the magnetic field distributions for normal driving. In

the same way, we compute the distribution of the normal gravity sensor measurements using the gravity sensor measurement model described earlier in this section. Using these generated normal sensor data, we train the one-class SVM classifier, which is then used for off-wheel detection.

6 SAFE DRIVING MONITORING APPLICATION DESIGN

We will present the safe driving monitoring applications including (1) manual/visual distraction, (2) Steering wheel control technique, (3) lane changing/turning, and (4) fatigue motion detection. The workflow of MagTrack goes as follows. After collecting sensor data for a short time window W, the off-wheel detection algorithm is executed to detect whether either hand of the driver is not holding the steering wheel. If the driver is holding the steering wheel with both hands, then using the smartwatch onboard accelerometer and gyroscope, the left hand tracking algorithm is executed, and any steering motions are recorded. If the left hand is not steering the wheel, then the Simultaneous Tracking and Classification algorithm is executed to track both the right hand positions on the steering wheel and the head turn angles. The bimanual motions on the steering wheel, head turn angles, and off-wheel detection results are recorded in an event log, which is used to detect various unsafe behaviors.

Manual Distraction Detection. During driving, the driver should spend most of their time holding the steering wheel with both hands, except for short activities such as adjusting AC or switching radio stations. During each time interval W, MagTrack will firstly detect manual distractions using the algorithm described in Section 5. A manual distraction alert is issued if the driver spends more than T_f (typically 5) seconds with a hand off the steering wheel.

Bimanual Steering Control Monitoring. *Steering Technique Recognition:* The National Highway Traffic Safety Administration (NHTSA) recommends the push/pull steering technique [32, 37, 42, 43]. The major benefit is its ability to avoid injuries caused by airbag explosions in car accidents, while still maintaining the steering speed and flexibility. In the push/pull steering process, a driver uses one hand to push up the wheel, the other to slide up, grasp the wheel, and pull down to turn. The driver should hold the area of the steering wheel between 11 and 8 o'clock with their left hand and between 1 and 4 o'clock with their right hand regardless of the direction of the turn. Other steering techniques, such as hand-over-hand and single hand steering, should be used only when the car is moving slowly [43]. When using the hand-over-hand steering technique, the driver starts with hands at 9 and 3 o'clock. Depending on the direction the driver is turning, one hand will push the wheel up, while the other hand will let go, reach across the other arm, grasp the wheel and pull up.

MagTrack differentiates these steering techniques using the hand tracking algorithm described in Section 5. In this algorithm, the real-time hand positions for the left and right hand, represented by α and θ_1, are computed. When the driver is using the push/pull steering technique, the values of α and θ_1 are changing within the range $(-30°, 60°)$. Otherwise, α and θ_1 are within $(-30°, 180°)$ if the driver is using the hand-over-hand technique. Therefore, MagTrack detects the hand-over-hand technique by comparing α

Figure 9: Some Steering Wheel Holding Techniques.

and θ_1 with thresholds. When the hand positions have large values, the hand-over-hand technique is detected. Otherwise, the push/pull technique is detected.

Steering Wheel Holding Style Detection: NHTSA recommends that the drivers put their hands at the 3 and 9 o'clock positions [1, 43]. This is illustrated in the leftmost graph of Figure 9. Some other holding techniques, such as 2-10 o'clock or 4-8 o'clock holding (third and fourth in Figure 9), are detected by tracking the driver's bimanual positions, which are described in Section 5 and Section 3. Other improper holding styles, such as single-hand holding (second figure in Figure 9) and holding the wheel from the inner ring (fifth figure in Figure 9), will be detected by the off-wheel detection algorithm. If the driver maintains incorrect steering wheel control for a period longer than a threshold, then an alert will be sent to the driver.

Visual Distraction Detection. If the driver is detected to be holding the steering wheel with both hands, the head motions will be monitored using the algorithm described in Section 3.2. If the driver turns their head for a period longer than T_h (typically 5) seconds, then a visual distraction event is detected and an alert will be sent to the driver. If the driver turns back within T_h seconds, it indicates that the driver is observing the blind spots or side mirrors, and this information will be recorded and used in safe lane changing monitoring.

Safe Turning/Lane Changing. The driver needs to switch on the turn signal to notify the nearby vehicles and turn their head to observe the blind spots before steering the vehicle for a lane change or at an intersection for safety. MagTrack continuously monitors head turns using the algorithm described in Section 3.2. It also detects turn signals by monitoring the turn signal sounds using the matched filter [9]. When steering is detected, MagTrack checks the record for the previous W seconds. If either a head turn event or a turn signal event is missing, it will send an unsafe turning /lane changing alert to the driver.

When driving on a curvy road, the driver needs to frequently maneuver the steering wheel in motions similar to lane changing. We resolve this problem by using GPS on the smartphone to recognize the curvy roads. MagTrack will temporarily disable the turning/lane changing monitoring module to reduce false alarms.

Fatigue Motion Detection. Using MagTrack, we detect two types of motion, the head nodding [25, 30, 48, 51] and aggressive steering [19, 56], that are associated with drowsy driving. Using the algorithm described in Section 3.2, we detect the head nodding motions (head down turn). If the driver nods their head frequently, then it is likely the driver is drowsy and not safe. MagTrack compares the time interval between two consecutive head nods to a threshold T_d, and alerts the driver if the interval is smaller than T_d. Guided by previous research on drowsy driving monitoring [25], we set the value of T_d to be 5 seconds.

The rapid steering wheel movements are also shown to be correlated with fatigue driving [56]. Based on the left hand position tracking results, we estimate the rotation rate. If the rotation rate
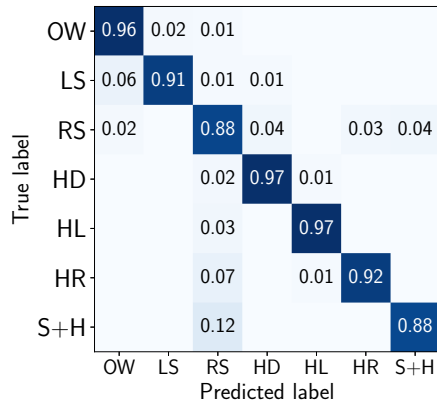
Figure 10: Driving Motion Type Confusion Matrix

exceeds T_r, then an alert will be sent to the driver. Based on [56], we set T_r to be 125 degrees/second.

7 EVALUATION

7.1 Driving Motion Recognition

Driving Motion Recognition Confusion Matrix. We first evaluate the motion classification performance of MagTrack. While driving slowly in a vacant parking lot, the driver conducts various driving motions, including off wheel (OW) motions (e.g., eating, controlling radio, texting, etc), steering using left hand (LS), steering using right hand (RS), head nodding (HD), head left turn (HL), head right turn (HR), and concurrent right hand steering and head turn (S+H). The recognition results are shown in Figure 10.

Overall, MagTrack can differentiate these driving motions accurately with the recognition accuracies around 0.9 or more for most types. The detection precision for concurrent right hand steering and head turn (S+H) is relatively high at 0.88. Closer examination of the algorithm reveals that the motion likelihood for S+H remains low when either the hand or the head is moving. This shows that by limiting the ranges of the state variables, we can ensure that the concurrent motion Kalman filter is activated only when both tags have large motions. Sometimes the concurrent motion Kalman filter can't track the motions accurately due to the large search space (three independent variables in the state vector). In these cases, the algorithm will falsely assign higher likelihood values to the right hand steering motion type, causing a 12% false detection rate.

In the experiments, RS get confused with HR from time to time. Specifically, 3% of RS are falsely recognized as HR, while 7% of HR are recognized as RS. A closer look at the sensing results shows that there are similarities between the magnetic field changes during right hand steering (RS) and head right turns (HR), especially when the right steering angle is small. To mitigate this problem, when conducting steering monitoring in the driving activity recognition, we design the algorithm to rely on tracking results for both left and right hands. Since the tracking for each hand uses different sensors (accelerometer and gyroscope for the left hand, and magnetometer for the right hand), the overall steering detection accuracy is higher than the motion tracking when only one sensor is used.

The head turn motion monitoring is relatively accurate. We achieved 97%, 97%, and 92% of detection precision for the three head turn directions: down, left and right, respectively.
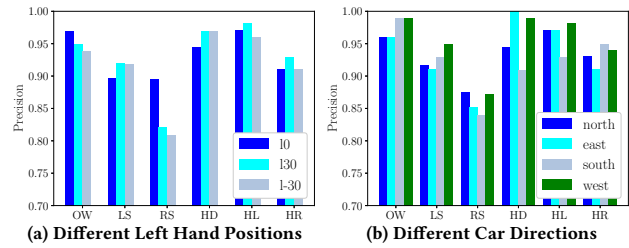

(a) Different Left Hand Positions   (b) Different Car Directions

Figure 11: Motion Type Classification Robustness

Driving Motion Recognition Robustness. To test the robustness of the motion classification algorithm, we test the algorithm under different settings. We firstly test the performance when the left hand holding position α is $0°$ (9 o'clock), $30°$ (10 o'clock) and $-30°$ (8 o'clock), and motion classification precision results are shown in Figure 11a. The recognition precision for the head turn motions, i.e., HD, HL, and HR, remains almost unchanged. This shows that the sensor measurement rotation algorithm described in Section 4 effectively reduces the impact of sensor orientation changes caused in holding position variation. However, RS detection accuracy degrades when the driver holds 30 or -30 degree positions. The reason is that the change of relative positions influences the sensor measurement model when the holding position changes. In this work, we focus on the cases when the driver holds the steering wheel at the 3-9 o'clock positions during driving. To adapt to other steering wheel holding style, such as 2-10 o'clock holding positions, we need to adjust the sensor measurement model parameters using the calibration process described in Section 3.1.

We also test the system robustness by dividing the car moving directions into four categories based on corresponding GPS data. Shown in Figure 11b, MagTrack maintains similar motion recognition accuracy regardless of the car's moving direction, proving the effectiveness of the geomagnetic field reduction algorithm described in Section 4.

The vehicle itself also generates a magnetic field during their operations [49]. For example, in our experiments, we found that braking generates a magnetic field of about 5 μT on the smartwatch magnetometer. To test its impact, we collected 10 data segments with braking, and ran the MagTrack algorithm on them. The results showed that the changes of MagTrack tracking angles due to braking were small, and no false alarms were created.

7.2 Unsafe Driving Activity Detection

Dataset. The dataset contains two parts: the controlled driving and the uncontrolled free driving datasets. We collect the controlled driving data on vacant roads and parking lots. A co-pilot observes surroundings to ensure the emptiness of the roads, then the driving and data collection begin. The co-pilot records labels and starting time of the driver's driving behaviors into the dataset. The experiments are conducted in eight cars of the following models: Ford Fusion, Honda Civic, Toyota RAV4, Honda Accord, Ford Focus, and Nissan Altima. We have recruited 10 volunteers, and each conducts the following unsafe driving activities multiple times: turning/lane changing without head turns or turn signal, turning with incorrect steering techniques, and visual distractions. To collect safe driving data, the drivers also conduct safe turning/lane changing, where the drivers observe blind spots and switch on the turn signals before

Events	# TP	# FP	# GT	PR	RC
Unsafe Turn, Lane Change	84	13	100	0.87	0.84
Incorrect Steering Control	88	7	95	0.92	0.92
Manual Distraction	131	11	148	0.92	0.89
Visual Distraction	105	19	116	0.85	0.91
Fatigue Driving Motions	85	11	88	0.88	0.96
Overall			547	0.87	0.90

Table 1: Unsafe Driving Activity Detection Result

steering the wheel using the correct technique. For the manual distraction data, the drivers conduct six types of distraction activities, including controlling the radio, texting, eating, one-handed driving with either left or right hand for 2 minutes each. For fatigue driving data, the drivers either nod head frequently, or steer wheel quickly for a short period of time. In total, we have collected 500+ instances of unsafe driving data.

We collect uncontrolled data when the drivers are driving with regular traffic. The drivers are asked to focus on safety so that only a few incorrect driving behaviors are recorded. A co-pilot collects ground truth of the driver's wheel holding positions, steering techniques and head turns. In total, we have more than 250 minutes of uncontrolled driving data for system evaluation.

Overall Detection Results. Table 1 provides the detection precision (PR) and recall rate (RC) for the tested unsafe driving scenarios, which includes both the normal driving dataset and the controlled unsafe driving dataset. PR is defined as $TP/(TP + FP)$, and RC is defined as $TP/(TP + FN)$, where TP represents True Positive, FP represents False Positive, and FN represents False Negative. Overall, there are 547 instances of Ground Truth (GT) unsafe driving events. MagTrack detects these events with a precision of 0.87 and a recall rate of 0.90, respectively.

We can also see that the detection precision and recall rate for unsafe turn/lane changing are 0.87 and 0.84, respectively. This shows the feasibility for MagTrack to synthesize the information from hand tracking, head turn monitoring and turn signal detection modules effectively in order to monitor the entire process of turning and lane changing.

The detection precision and the recall rate for incorrect steering technique are both 0.92. One source of error is the driver's complex variations in the steering technique on the road. For example, when steering with the push/pull technique, the driver sometimes steers the wheel with asymmetric motions, with one hand moving with a larger angle and the other with a smaller one. In these cases, MagTrack detects large hand holding position changes and tends to falsely predict a hand-over-hand technique. One way to address this issue is to include more types of steering techniques into the system with details of corresponding motions. In this work, we focus on the recognition of two popular steering techniques.

The detection precision of manual distraction detection is 0.92, and the recall rate is 0.89. One major source of errors is that MagTrack sometimes confuses manual distractions with some low holding positions, because the magnetic fields at the magnetometer in
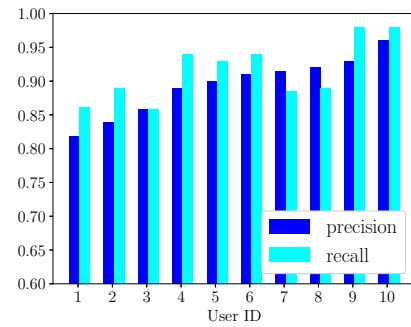
Figure 12: Detection Accuracy for Individual Users

both cases are weak. This can be improved if we use a stronger magnet on the hand.

The visual distraction detection algorithm has a recall rate of 0.91, meaning that most visual distractions are detected. This demonstrates the smartwatch magnetometer's high sensitivity in detecting head motions. However, precision is lower at 0.85. The main reason is that several other types of head motions are not recognized by MagTrack during driving. For example, when viewing the rear mirrors, the driver can lower his or her head and have small back-forth head motions. On uneven roads, the driver's head and hand can have up-down vibrations. To mitigate these false alarms, we can explore additional head motion models in the future, so that motions other than head left, right and down turns can be recognized by the system. Furthermore, the algorithm sometimes confuses the head turn motions with steering motions, which can also cause false detection.

Our algorithm achieves a high recall rate of 0.96 to detect fatigue driving motions. This is partly because of the reliability to detect head nodding motions. We find that head nodding can create strong and distinguishable patterns in the magnetic sensor measurements. In addition, the aggressive steering detection based on smartwatch IMUs is also robust and accurate. However, a few false alarms are detected because MagTrack confuses normal steering with aggressive steering. False alarms happen more often if the driver steers with the hand-over-hand technique. The rotation rate of the steering wheel is high so that MagTrack sometimes falsely recognizes it as aggressive steering motions.

Comparison Against Camera-based Solution. We road-tested a few mobile camera-based driver monitoring apps, including Drivelert, Sleepiness Warning, DriveAwake, Driver Fatigue, and Fatigue and Eye Blink Detection. These apps did not work in dark environments, e.g., driving at night, because they have difficulty capturing useful photos under low-light conditions.

In terms of detection accuracy, we compared a recent system that uses a camera to monitor the driver's head turns [3]. This solution achieved an accuracy of 97.5% in differentiating down, front, and up head turns, and 98.2% in differentiating left, front, and right head turns. MagTrack achieves 98% accuracy in detecting different head poses: front, left, right, and down head turn motions.

Detection Accuracy for Individual Users. We further analyze the unsafe activity detection accuracy for each driver, and the results are shown in Figure 12. We can see that although individual variations exist, MagTrack can maintain an overall accurate detection performance. Among different drivers, the detection precision

ranges from 0.82 to 0.96, while the detection recall rate ranges from 0.86 to 0.98.

7.3 Energy Consumption

MagTrack is implemented and tested on Android Wear. The application level functions of MagTrack are running on the driver's smartphone, while sensing, signal processing, and motion tracking functions are executed on the smartwatch. Specifically, MagTrack continuously collects the uncalibrated magnetic sensor and gravity sensor data at 50Hz, then conducts the simultaneous tracking and classification algorithm to recognize driving motions on the smartwatch.

We tested the battery life of the smartwatch using three fully charged Samsung Gear Live smartwatches and recorded the remaining battery life after 1, 3, and 6 hours. On average, the remaining battery life is 93%, 78%, and 62%, respectively. We project that the battery life drops about 7% every hour, and the total battery life is about 14 hours. In comparison, the battery life drops around 1% when the watch is idle. We note a more sophisticated implementation with adaptive sampling rates may significantly reduce the energy consumption of MagTrack.

7.4 User Study

We conducted a user study on all 10 volunteers about the experience of using MagTrack. 3 users felt the added magnetic tags are heavy, while others felt OK about the additional weight. Some volunteers suggested that the hand magnet can be attached on a glove or a bracelet/wristband, and the head magnet can be attached to a cap because they used these accessories anyway.

8 DISCUSSION

8.1 Multi-wearable Designs and Applications.

As wearable sensing and computing technologies become mature, activity tracking using multiple wearables or tags is not new. There are research prototypes ranging from body sensor networks to medical IoT [5, 14, 21, 24, 28, 41] and to commercially available products [8, 17, 31] for a wide range of applications, including health monitoring, sports, entertainment, and scientific explorations. For safety-critical applications like law enforcement and firefighting, wearables also show a promising future [17, 76]. In terms of driving applications, there are ear-worn head nodding detectors [4]. Particularly, previous work [7] used two smartwatches and a smartphone to monitor manual distractions. Compared to such multi-wearable designs, our system has three unique advantages: first, the magnetic tags are low cost and they don't require battery recharge. Second, MagTrack only needs one magnetometer to track multiple tags, the system is simple and efficient. Third, wearable magnetic tags have the potential to become more user-friendly and non-intrusive.

We demonstrated several types of wearable magnetic tags in Figure 13. These proof of concept designs are preliminary and have space to improve. First, smaller but stronger magnets can be used. With Neodymium-Iron-Boron magnets of stronger grades, MagTrack will achieve the same tracking accuracy with a smaller magnet. Second, more sensitive magnetic sensors may improve the sensing range and accuracy as well.

| (a) Wrist Band | (b) Ring | (c) Glove |

| (d) Hat | (e) Head Band | (f) Eye-glass |

Figure 13: Sample Magnetic Wearable Designs

Many people can benefit from our design. For example, driving couches can use MagTrack to train and improve behaviors for new drivers [15, 61]; insurance companies can use MagTrack to monitor driving habits in order to achieve more accurate risk assessment and insurance premium adjustment [52]. Furthermore, many drivers with special needs can benefit from MagTrack. Research show distraction detection systems can improve safety for drivers with Attention Deficit and Hypoactivity Disorder (ADHD) [55, 61]. The system can also help night commuters and long-distance truck drivers by alerting fatigue driving motions including head nodding and sudden aggressive steering.

Novel Applications. Besides driving monitoring, MagTrack can be used to monitor a class of activities where coordinated bimanual and head motions are involved. Existing monitoring systems are often limited because they rely on a single smartwatch, which can only monitor one hand. For example, doctors have been using smartwatches to monitor eating activities for patients with diabetes and heart diseases in order to control food intake [40, 77]. An existing system has demonstrated good recognition accuracy [57], but it is limited to monitoring eating with a single hand, and it cannot monitor eating activities that involve the other hand, such as eating with a fork and knife. MagTrack can monitor bimanual eating gestures by attaching additional magnetic tags to the other hand. In addition, head gestures during eating can also be captured, which can help distinguishing eating from other activities at the dining table.

Similarly, existing hand washing monitoring systems also suffer from a lack of bimanual motion monitoring. Systems that use a single smartwatch are insufficient in achieving highly accurate hand washing monitoring [65]. While using two smartwatches can improve monitoring accuracy, it introduces high cost to the users [20]. MagTrack can be used to monitor bimanual hand washing motions, with only one additional low-cost magnetic tag.

There are many other medical applications that involve coordinated bimanual and head motions that can potentially benefit from MagTrack, such as hand-eye coordination skill assessment [63], which helps to detect development disorders in young children and to detect cognitive ability degeneration in elderly people. Another example is the monitoring of wrist injury recovery exercises [45], which involve well-defined motions of the user's wrist joint.

8.2 Lesson Learned

Driving Context Integration. MagTrack is able to monitor a wide range of unsafe driving behaviors. However, it does not cover some

other factors associated with driving risks, such as car speed, sudden acceleration or braking, weather, traffic and road conditions. These factors can be integrated into MagTrack, if such information is available in real-time.

We will explore adding new safe driving monitoring scenarios by including different driving contexts. For example, by combining the driving speed context with the steering wheel control monitoring, MagTrack can detect aggressive driving. By combining the in-car conversation context [35] with head turn monitoring, distractions due to conversations can be better detected.

User Variations. Every driver has a personal sitting posture, height, and steering wheel holding habits, etc. MagTrack can be calibrated based on these factors. Specifically, we have observed that the position of the smartwatch on the user's wrist is an important factor, as well as the driver's sitting posture. The distance between the head magnet and the smartwatch also matters. Therefore, we estimate these factors for each driver and calibrate the sensing models accordingly.

MagTrack has been tested for right-handed drivers. However, MagTrack can still work if the driver is left-handed and prefers to wear a smartwatch on the right hand. The driver just needs to put the magnetic tag on the left hand. In the US, the radio, transmission gear, cup holder, etc are all on the right hand side of the driver. Therefore, wearing a smartwatch on the right hand actually makes tracking easier, because we can take advantages of IMU sensors on the smartwatch to track right hand activities more accurately.

9 STATE OF THE ART

Driving Monitoring: Cameras have been used to monitor the driver's head motions, enabling drowsy driving and visual distraction detection [27, 36, 59, 66, 71, 73]. There are a few advantages of camera systems over MagTrack: they do not require wearables on the users, and the eyelid movements can be recognized. However, MagTrack provides its unique benefits. Firstly, MagTrack works under low-light and all weather conditions when cameras have difficulty capturing images [9]. Secondly, some people have privacy concerns about camera-based solutions. There is a trade-off between safety and convenience in terms of safe driving monitoring. Although some users feel the need for wearing devices burdensome, others are more open to additional gadgets, which is demonstrated by the popularity of wearable driving monitoring devices on the market [4, 39, 50, 62, 64].

Earlier inertia-sensor-based safe driving monitoring systems mainly focus on monitoring car motion dynamics and can alert abnormal vehicle movements, such as aggressive acceleration or turning [9, 38, 72, 74, 75]. However, they often leave insufficient time for the drivers to respond to complex road situations, especially when the drivers are distracted. Using the battery-free magnetic tags and smartwatch sensors, MagTrack enables early detection of dangerous driving behaviors, including distracted driving, unsafe lane changing/turning, and incorrect steering techniques.

Fatigue driving detection is an ongoing research problem, and many techniques have been used trying to solve it, including eyelid closure detection [73], head nodding detection [25, 30, 48, 51], aggressive steering detection [19, 56], abnormal ECG and respiratory patterns detection, etc. Eyelid closure detection systems are popular, but they have poor performance under low-light conditions.

Furthermore, studies show that many micro-sleeps during driving occur with the driver's eyes open [13]. Some systems rely on head nodding detection using different sensors, such as specialized capacitive sensors [30], and IMU sensors worn on the head [4, 39]. In comparison, MagTrack detects head nodding motions with only a low cost magnetic tag on the head and a smartwatch on the wrist, and yet achieves high accuracy. MagTrack also detects aggressive steering motions that can indicate fatigue driving.

Simultaneous Tracking and Classification: STC was initially proposed to solve the target tracking and classification in the radar monitoring scenario [26, 46, 47, 53]. The basic idea is to use the special feature metrics to infer the target type. For example, it is possible to infer the aircraft model based on its flight speed and acceleration [47]. However, in our problem setting, sometimes the two magnetic tags move at the same time, which poses a new and unique challenge. To address this problem, we define additional "virtual" motion types that represent the concurrent motions of the two magnetic tags, and use the STC framework to detect such concurrent types based on the corresponding sensor measurement patterns.

Magnetic Sensing: The free motions of each magnetic tag have 6 degrees of freedom: 3 degrees of position and 3 degrees of orientation. Previous research typically require at least two 3-axis magnetometers to track each free-moving magnet [10, 12, 16, 23, 60]. On the other hand, a single magnetometer can obtain a qualitative description of the magnetic field, such as the transportation states [11, 54]. Our case, where only one magnetometer is used to track two magnetic tags, is different from all these works. Our perspective is that the driving motions have constraints: the hands are constrained to the steering wheel, while the head is constrained by the car seat. We analyze the hand and head motion constraints, and construct detailed motion and sensing models, then use the Kalman filtering algorithms to track motions with high accuracy.

10 CONCLUSION

We built MagTrack that can reliably monitor both a driver's bimanual and head motions in real-time. Compared to existing solutions, MagTrack has four major benefits: 1) it uses battery-free low-cost magnetic accessories for active tracking, and our system is robust against different types of vehicles and environmental settings; 2) a novel sensing algorithm can track two tags with only a single magnetometer on a smartwatch, because each tag has its unique motion patterns and constraints; 3) the tracking results of hand and head motions can be used in learning based algorithms to detect a wide range of unsafe driving activities, including manual and visual distractions, incorrect steering techniques, and unsafe turning and lane changing; 4) it achieves high monitoring accuracy. In 500+ minutes road tests with 500+ instances of driving activities and 10 participants, MagTrack detects unsafe driving activities with 87% of precision and 90% of recall rate, demonstrating the potential of magnetic wearables based activity recognition.

REFERENCES

[1] AAA 2017. Avoiding Crashes and Emergency Maneuvers. http://seniordriving.aaa.com/improve-your-driving-skills/handle-unexpected-situations/avoiding-crashes-emergency/.

[2] N. Aksan, L. Sager, S Hacker, Marini R., Dawson J., Anderson S., and Rizzo M. 2016. Forward Collision Warning: Clues to Optimal Timing of Advisory Warnings. In *SAE International Journal of Transportation Safety*.

[3] Nawal Alioua, Aouatif Amine, Alexandrina Rogozan, Abdelaziz Bensrhair, and Mohammed Rziza. 2016. Driver head pose estimation using efficient descriptor fusion. *EURASIP Journal on Image and Video Processing* 2016, 1 (2016), 2.

[4] Amazon. 2019. Driver Alertness System. https://www.amazon.com/dp/B00NAQOVF6/ref=psdc_7459508011_t1_B004F2OEEM.

[5] Takashi Aoki, Jonathan Feng-Shun Lin, Dana Kulić, and Gentiane Venture. 2016. Segmentation of human upper body movement using multiple IMU sensors. In *2016 38th Annual International Conference of the IEEE Engineering in Medicine and Biology Society (EMBC)*. IEEE, 3163–3166.

[6] Frederick J Berg, Timothy J Bennett, Alan C Davis, Richard K Riefe, Ronald H Dybalski, and Timothy M Phillips. 2007. Steering system with haptic driver warning. US Patent 7,280,046.

[7] Chongguang Bi, Jun Huang, Guoliang Xing, Landu Jiang, Xue Liu, and Minghua Chen. 2017. SafeWatch: A Wearable Hand Motion Tracking System for Improving Driving Safety. In *Proceedings of the Second International Conference on Internet-of-Things Design and Implementation (IoTDI '17)*. ACM, New York, NY, USA, 223–232. https://doi.org/10.1145/3054977.3054979

[8] BioStamp. 2019. BioStamp Wearables Health Monitoring. https://www.mc10inc.com.

[9] Dongyao Chen, Kyong-Tak Cho, Sihui Han, Zhizhuo Jin, and Kang G. Shin. 2015. Invisible Sensing of Vehicle Steering with Smartphones. In *Proceedings of the 13th Annual International Conference on Mobile Systems, Applications, and Services (MobiSys '15)*. ACM, New York, NY, USA, 1–13. https://doi.org/10.1145/2742647.2742659

[10] Ke-Yu Chen, Kent Lyons, Sean White, and Shwetak Patel. 2013. uTrack: 3D input using two magnetic sensors. In *Proceedings of the 26th annual ACM symposium on User interface software and technology*. ACM, 237–244.

[11] Ke-Yu Chen, Rahul C Shah, Jonathan Huang, and Lama Nachman. 2017. Mago: Mode of Transport Inference Using the Hall-Effect Magnetic Sensor and Accelerometer. *Proceedings of the ACM on Interactive, Mobile, Wearable and Ubiquitous Technologies* 1, 2 (2017), 8.

[12] Chihwen Cheng, Xueliang Huo, and Maysam Ghovanloo. 2009. Towards a magnetic localization system for 3-D tracking of tongue movements in speech-language therapy. In *Engineering in Medicine and Biology Society, 2009. EMBC 2009. Annual International Conference of the IEEE*. IEEE, 563–566.

[13] In-Ho Choi, Chan-Hee Jeong, and Yong-Guk Kim. 2016. Tracking a driver's face against extreme head poses and inference of drowsiness using a hidden Markov model. *Applied Sciences* 6, 5 (2016), 137.

[14] Ashraf Darwish and Aboul Ella Hassanien. 2011. Wearable and implantable wireless sensor network solutions for healthcare monitoring. *Sensors* 11, 6 (2011), 5561–5595.

[15] Kamal El Farouki, Emmanuel Lagarde, Ludivine Orriols, Manuel-Pierre Bouvard, Benjamin Contrand, and Cédric Galéra. 2014. The increased risk of road crashes in attention deficit hyperactivity disorder (ADHD) adult drivers: driven by distraction? Results from a responsibility case-control study. *PLoS one* 9, 12 (2014), e115002.

[16] Aydin Farajidavar, Jacob M Block, and Maysam Ghovanloo. 2012. A comprehensive method for magnetic sensor calibration: A precise system for 3-D tracking of the tongue movements. In *Engineering in Medicine and Biology Society (EMBC), 2012 Annual International Conference of the IEEE*. IEEE, 1153–1156.

[17] Firehouse. 2019. Fire Technology. https://www.firehouse.com/tech-comm/mobile-technology-accessories/article/21000640/wearable-technology-for-firefighters.

[18] Center for Disease Control. 2019. Distracted Driving Statistics. https://www.cdc.gov/motorvehiclesafety/distracted_driving.

[19] Pia M Forsman, Bryan J Vila, Robert A Short, Christopher G Mott, and Hans PA Van Dongen. 2013. Efficient driver drowsiness detection at moderate levels of drowsiness. *Accident Analysis & Prevention* (2013).

[20] Valerie Galluzzi, Ted Herman, and Philip Polgreen. 2015. Hand Hygiene Duration and Technique Recognition Using Wrist-worn Sensors. In *Proceedings of the 14th International Conference on Information Processing in Sensor Networks (IPSN '15)*. ACM, New York, NY, USA, 106–117. https://doi.org/10.1145/2737095.2737106

[21] Mostafa Haghi, Kerstin Thurow, and Regina Stoll. 2017. Wearable devices in medical internet of things: scientific research and commercially available devices. *Healthcare informatics research* 23, 1 (2017), 4–15.

[22] Brett O Hall. 2001. Collision avoidance system. US Patent 6,223,125.

[23] Xinying Han, Hiroaki Seki, Yoshitsugu Kamiya, and Masatoshi Hikizu. 2010. Wearable handwriting input device using magnetic field: 2nd report: Influence of misalignment of magnet and writing plane. *Precision Engineering* 34, 3 (2010), 425–430.

[24] Mark A Hanson, Harry C Powell Jr, Adam T Barth, Kyle Ringgenberg, Benton H Calhoun, James H Aylor, and John Lach. 2009. Body area sensor networks: Challenges and opportunities. *Computer* 42, 1 (2009), 58–65.

[25] Qichang He, Wei Li, Xiumin Fan, and Zhimin Fei. 2016. Evaluation of driver fatigue with multi-indicators based on artificial neural network. *IET Intelligent Transport Systems* 10, 8 (2016), 555–561.

[26] Kasthuri Jayarajah, Vigneshwaran Subbaraju, Noel Athaide, Lakmal Meeghapola, Andrew Tan, and Archan Misra. 2018. Can multimodal sensing detect and localize transient events?. In *Ground/Air Multisensor Interoperability, Integration, and Networking for Persistent ISR IX*, Vol. 10635. International Society for Optics and Photonics, 106351A.

[27] Qiang Ji and Xiaojie Yang. 2002. Real-time eye, gaze, and face pose tracking for monitoring driver vigilance. *Real-Time Imaging* 8, 5 (2002), 357–377.

[28] Haojian Jin, Zhijian Yang, Swarun Kumar, and Jason I Hong. 2018. Towards wearable everyday body-frame tracking using passive rfids. *Proceedings of the ACM on Interactive, Mobile, Wearable and Ubiquitous Technologies* 1, 4 (2018), 145.

[29] Derick A Johnson and Mohan M Trivedi. 2011. Driving style recognition using a smartphone as a sensor platform. In *Intelligent Transportation Systems (ITSC), 2011 14th International IEEE Conference on*. IEEE, 1609–1615.

[30] Philip W Kithil, Roger D Jones, and John McCuish. 2001. *Driver alertness detection research using capacitive sensor array*. Technical Report. SAE Technical Paper.

[31] Klic. 2019. Klic Wearables. (2019). https://www.klik.co/en/wearables.

[32] T. J. Kline. 2007. Using Efficient Steering Techniques. *Journal of traffic safety education* 55, 1 (2007), 14–16, 22. http://dx.doi.org/

[33] Dong-Min Lee. 2001. Method for detecting lane deviation of vehicle. US Patent 6,317,057.

[34] John Lee, Daniel McGehee, Timothy Brown, and Michelle L Reyes. 2002. Collision Warning Timing, Driver Distraction, and Driver Response to Imminent Rear-End Collisions in a High-Fidelity Driving Simulator. *Human factors* (2002).

[35] Youngki Lee, Chulhong Min, Chanyou Hwang, Jaeung Lee, Inseok Hwang, Younghyun Ju, Chungkuk Yoo, Miri Moon, Uichin Lee, and Junehwa Song. 2013. Sociophone: Everyday face-to-face interaction monitoring platform using multi-phone sensor fusion. In *Proceeding of the 11th annual international conference on Mobile systems, applications, and services*. ACM, 375–388.

[36] Kun Li, Man Lu, Fenglong Lu, Qin Lv, Li Shang, and Dragan Maksimovic. 2012. Personalized driving behavior monitoring and analysis for emerging hybrid vehicles. In *International Conference on Pervasive Computing*. Springer, 1–19.

[37] BOTTOM LINE. 2012. *Get with the times: You're driving all wrong.* https://www.nbcnews.com/businessmain/get-times-youre-driving-all-wrong-518710/.

[38] Luyang Liu, Hongyu Li, Jian Liu, Cagdas Karatas, Yan Wang, Marco Gruteser, Yingying Chen, and Richard P Martin. 2017. Bigroad: Scaling road data acquisition for dependable self-driving. In *Proceedings of the 15th Annual International Conference on Mobile Systems, Applications, and Services*. ACM, 371–384.

[39] Maven Machine. 2019. Maven co-pilot. https://mavenmachines.com/maven-co-pilot.

[40] Chinmay Manohar, James A Levine, Debashis K Nandy, Ahmed Saad, Chiara Dalla Man, Shelly K McCrady-Spitzer, Rita Basu, Claudio Cobelli, Rickey E Carter, Ananda Basu, et al. 2012. The effect of walking on postprandial glycemic excursion in patients with type 1 diabetes and healthy people. *Diabetes Care* 35, 12 (2012), 2493–2499.

[41] Uwe Maurer, Asim Smailagic, Daniel P Siewiorek, and Michael Deisher. 2006. *Activity recognition and monitoring using multiple sensors on different body positions*. Technical Report. Carnegie-Mellon Univ, Pittsburgh, PA, USA.

[42] State Farm Insurance. 2017. *Things Have Changed Since You Learned to Drive.* https://www.statefarm.com/simple-insights/auto-and-vehicles/things-have-changed-since-you-learned-to-drive.

[43] Texas Driver Training Division, Texas Driver License Division. 2016. *Behind-the-Wheel Instruction Guide*.

[44] John McDonald. 18-7-2006. Rotation About an Arbitrary Axis. In *CGEMS - Computer Graphics Educational Materials*, (Ed.). The Eurographics Association. https://doi.org/10.2312/cgems04-11-1367

[45] Summit Medical. 2019. Wrist Injury Recovery Exercises. https://www.summitmedicalgroup.com/library/adult_health/sma_wrist_tendonitis_exercises/.

[46] Wei Mei, Gan-Lin Shan, and X Rong Li. 2007. Simultaneous tracking and classification: a modularized scheme. *IEEE transactions on aerospace and electronic systems* 43, 2 (2007).

[47] Michael I Miller, Anuj Srivastava, and Ulf Grenander. 1995. Conditional-mean estimation via jump-diffusion processes in multiple target tracking/recognition. *IEEE Transactions on Signal Processing* 43, 11 (1995), 2678–2690.

[48] Erik Murphy-Chutorian and Mohan Manubhai Trivedi. 2010. Head pose estimation and augmented reality tracking: An integrated system and evaluation for monitoring driver awareness. *IEEE Transactions on intelligent transportation systems* 11, 2 (2010), 300–311.

[49] Phuc Nguyen, Hieu Nguyen, Dong Nguyen, Thang N Dinh, Hung M La, and Tam Vu. 2017. ParkSense: automatic parking positioning by leveraging in-vehicle magnetic field variation. *IEEE Access* 5 (2017), 25021–25033.

[50] OptAlert. 2019. OptAlert. https://www.optalert.com/explore-products/scientifically-validated-glasses-mining.

[51] Jean Christophe Popieul, Philippe Simon, and Pierre Loslever. 2003. Using driver's head movements evolution as a drowsiness indicator. In *Intelligent Vehicles Symposium, 2003. Proceedings. IEEE*. IEEE, 616–621.

[52] Progressive. 2019. Snapshot Driving Monitor. https://www.progressive.com/auto/discounts/snapshot/.

[53] Valentin Radu, Catherine Tong, Sourav Bhattacharya, Nicholas D Lane, Cecilia Mascolo, Mahesh K Marina, and Fahim Kawsar. 2018. Multimodal deep learning for activity and context recognition. *Proceedings of the ACM on Interactive, Mobile, Wearable and Ubiquitous Technologies* 1, 4 (2018), 157.

[54] Sasank Reddy, Min Mun, Jeff Burke, Deborah Estrin, Mark Hansen, and Mani Srivastava. 2010. Using mobile phones to determine transportation modes. *ACM Transactions on Sensor Networks (TOSN)* 6, 2 (2010), 13.

[55] Consumer Reports. 2019. How To Track Teen Driver. https://www.consumerreports.org/cro/magazine/2014/07/how-to-track-your-teen-driver/index.htm.

[56] David Sandberg and Mattias Wahde. 2008. Particle swarm optimization of feed-forward neural networks for the detection of drowsy driving. In *Neural Networks, 2008. IJCNN 2008.(IEEE World Congress on Computational Intelligence). IEEE International Joint Conference on*. IEEE, 788–793.

[57] Sougata Sen, Vigneshwaran Subbaraju, Archan Misra, Rajesh Krishna Balan, and Youngki Lee. 2015. The case for smartwatch-based diet monitoring. In *2015 IEEE international conference on pervasive computing and communication workshops (PerCom workshops)*. IEEE, 585–590.

[58] Santokh Singh. 2015. *Critical reasons for crashes investigated in the national motor vehicle crash causation survey*. Technical Report.

[59] Alexander V Smirnov, Alexey Kashevnik, Igor Lashkov, Olesya Baraniuc, and Vladimir Parfenov. 2016. Smartphone-based identification of dangerous driving situations: Algorithms and implementation.. In *FRUCT*. 306–313.

[60] Eleuthère Stathopoulos, V Schlageter, B Meyrat, Y Ribaupierre, and P Kucera. 2005. Magnetic pill tracking: a novel non-invasive tool for investigation of human digestive motility. *Neurogastroenterology & Motility* 17, 1 (2005), 148–154.

[61] Maria Staubach. 2009. Factors correlated with traffic accidents as a basis for evaluating Advanced Driver Assistance Systems. *Accident Analysis & Prevention* 41, 5 (2009), 1025–1033.

[62] Smartcap Technology. 2019. Smart Cap. http://www.smartcaptech.com/life-smart-cap.

[63] Simone Verheij, Danya Muilwijk, Johan J.M. Pel, Tischa J.M. van der Cammen, Francesco U.S. Mattace-Raso, and Johannes van der Steen. 2012. Visuomotor Impairment in Early-Stage Alzheimer's Disease: Changes in Relative Timing of Eye and Hand Movements. *Journal of Alzheimer's Disease* 30, 1 (2012), 131–143.

[64] Vigo. 2019. Vigo. https://www.wearvigo.com.

[65] Vitalacy. 2019. Hand Washing Monitoring. (2019). http://www.hyginex.com/.

[66] Esra Vural, Mujdat Cetin, Aytul Ercil, Gwen Littlewort, Marian Bartlett, and Javier Movellan. 2007. Drowsy driver detection through facial movement analysis. *Human–computer interaction* (2007), 6–18.

[67] Eric A Wan and Rudolph Van Der Merwe. 2000. The unscented Kalman filter for nonlinear estimation. In *Adaptive Systems for Signal Processing, Communications, and Control Symposium 2000. AS-SPCC. The IEEE 2000*. Ieee, 153–158.

[68] Yanxin Wang, Johnny Wong, and Andrew Miner. 2004. Anomaly intrusion detection using one class SVM. In *Proceedings from the Fifth Annual IEEE SMC Information Assurance Workshop, 2004*. IEEE, 358–364.

[69] Wikipedia. 2019. Kalman Filtering Basics. https://en.wikipedia.org/wiki/Kalman_filter#Details.

[70] Wikipedia. 2019. Maximum Likelihood Parameter Estimation. https://en.wikipedia.org/wiki/Maximum_likelihood_estimation.

[71] Jie Wu, Kun Li, Yifei Jiang, Qin Lv, Li Shang, and Yihe Sun. 2011. Large-scale battery system development and user-specific driving behavior analysis for emerging electric-drive vehicles. *Energies* 4, 5 (2011), 758–779.

[72] Minglin Wu, Sheng Zhang, and Yuhan Dong. 2016. A novel model-based driving behavior recognition system using motion sensors. *Sensors* 16, 10 (2016), 1746.

[73] Chuang-Wen You, Nicholas D. Lane, Fanglin Chen, Rui Wang, Zhenyu Chen, Thomas J. Bao, Martha Montes-de Oca, Yuting Cheng, Mu Lin, Lorenzo Torresani, and Andrew T. Campbell. 2013. CarSafe App: Alerting Drowsy and Distracted Drivers Using Dual Cameras on Smartphones. In *Proceeding of the 11th Annual International Conference on Mobile Systems, Applications, and Services (MobiSys '13)*. ACM, New York, NY, USA, 13–26. https://doi.org/10.1145/2462456.2465428

[74] Jiadi Yu, Zhongyang Chen, Yanmin Zhu, Yingying Jennifer Chen, Linghe Kong, and Minglu Li. 2017. Fine-grained abnormal driving behaviors detection and identification with smartphones. *IEEE Transactions on Mobile Computing* 16, 8 (2017), 2198–2212.

[75] Jiadi Yu, Hongzi Zhu, Haofu Han, Yingying Jennifer Chen, Jie Yang, Yanmin Zhu, Zhongyang Chen, Guangtao Xue, and Minglu Li. 2016. Senspeed: Sensing driving conditions to estimate vehicle speed in urban environments. *IEEE Transactions on Mobile Computing* 15, 1 (2016), 202–216.

[76] ZDNet. 2019. Wearable Cameras for the Police. https://www.zdnet.com/article/22000-london-police-are-getting-wearable-cameras-to-video-crime.

[77] Chiara Zecchin, Andrea Facchinetti, Giovanni Sparacino, Chiara Dalla Man, Chinmay Manohar, James A Levine, Ananda Basu, Yogish C Kudva, and Claudio Cobelli. 2013. Physical activity measured by physical activity monitoring system correlates with glucose trends reconstructed from continuous glucose monitoring. *Diabetes technology & therapeutics* 15, 10 (2013), 836–844.